HHS Public Access

Author manuscript

Neuropharmacology. Author manuscript; available in PMC 2017 September 01.

Published in final edited form as:

Neuropharmacology. 2016 September ; 108: 193–206. doi:10.1016/j.neuropharm.2016.04.031.

A clickable neurosteroid photolabel reveals selective Golgi compartmentalization with preferential impact on proximal inhibition

Xiaoping Jiang[*],
Department of Psychiatry, Washington University in St. Louis School of Medicine. St. Louis, MO USA 63110

Hong-Jin Shu[*],
Department of Psychiatry, Washington University in St. Louis School of Medicine. St. Louis, MO USA 63110

Kathiresan Krishnan,
Department of Developmental Biology, Washington University in St. Louis School of Medicine. St. Louis, MO USA 63110

Mingxing Qian,
Department of Developmental Biology, Washington University in St. Louis School of Medicine. St. Louis, MO USA 63110

Amanda A. Taylor,
Department of Psychiatry, Washington University in St. Louis School of Medicine. St. Louis, MO USA 63110

Douglas F. Covey,
Department of Developmental Biology, Department of Anesthesiology, Taylor Family Institute for Innovative Psychiatry Research, Washington University in St. Louis School of Medicine. St. Louis, MO USA 63110

Charles F. Zorumski, and
Department of Psychiatry, Department of Neuroscience, Taylor Family Institute for Innovative Psychiatry Research, Washington University in St. Louis School of Medicine. St. Louis, MO USA 63110

Steven Mennerick

Correspondence to: Steve Mennerick, Department of Psychiatry, Washington University School of Medicine, 660 S. Euclid Ave., Campus Box 8134, St. Louis, MO 63110, (314) 747-2988, menneris@wustl.edu.
[*]Contributed equally to the work.

Conflict of Interest statement: CFZ is a member of the Scientific Advisory Board for Sage Therapeutics, Inc., and CFZ and DFC hold equity in Sage Therapeutics. Washington University in St. Louis has licensed technology to Sage Therapeutics. The research herein was not supported by or licensed to Sage Therapeutics.

Department of Psychiatry, Department of Neuroscience, Taylor Family Institute for Innovative Psychiatry Research, Washington University in St. Louis School of Medicine. St. Louis, MO USA 63110

Abstract

Anesthetic, GABA-active neurosteroids potently augment $GABA_A$ receptor function, leading to important behavioral consequences. Neurosteroids and their synthetic analogues are also models for a wide variety of cell-permeant neuroactive compounds. Cell permeation and compartmentalization raise the possibility that these compounds' actions are influenced by their cellular partitioning, but these contributions are not typically considered experimentally or therapeutically. To examine the interplay between cellular accumulation and pharmacodynamics of neurosteroids, we synthesized a novel chemical biology analogue (bio-active, clickable photolabel) of GABA-active neurosteroids. We discovered that the analogue selectively photo-labels neuronal Golgi in rat hippocampal neurons. The active analogue's selective distribution was distinct from endogenous cholesterol and not completely shared by some non-GABA active, neurosteroid-like analogues. On the other hand, the distribution was not enantioselective and did not require energy, in contrast to other recent precedents from the literature. We demonstrate that the soma-selective accumulation can act as a sink or source for steroid actions at plasma-membrane GABA receptors, altering steady-state and time course of effects at somatic $GABA_A$ receptors relative to dendritic receptors. Our results suggest a novel mechanism for compartment-selective drug actions at plasma-membrane receptors.

Keywords

$GABA_A$ receptor; anesthetic; anxiolytic; inhibition; Golgi; synaptic

1. INTRODUCTION

Neurosteroids produced from cholesterol potently augment neuronal inhibition at $GABA_A$ receptors, and synthetic analogues have clinical potential as anxiolytics, anesthetics, anticonvulsants and neuroprotectants (Antkowiak, 2001; Belelli et al., 2006; Belelli and Lambert, 2005; Zorumski et al., 2000; Zorumski et al., 2013). Our previous work suggested that, likely because of their strong lipophilicity, fluorescent neurosteroid analogues accumulate inside cells (Akk et al., 2005; Li et al., 2007; Shu et al., 2004), but important aspects of the nature of this accumulation remain obscure.

Past work has shown that across a limited range of defined steroid structures, lipophilicity correlates with steroid potency and time course of steroid effects (Chisari et al., 2010; Chisari et al., 2009). When potency is measured as the aqueous concentration that generates a fraction of a drug's maximum effect, a misleading picture may emerge because the local lipid concentration, rather than aqueous concentration, may drive receptor interactions. The intracellular accumulation of fluorescent neurosteroid analogues suggests the possibility that cellular accumulation can also influence actions at $GABA_A$ receptors by altering the local membrane concentration relevant to receptors. However, specific compartmentalization, its

dependence on simple hydrophobic interactions versus more specific binding or uptake, and the physiological impact of any compartmentalization are incompletely understood.

Fluorescent analogues can alter the behavior of compounds and are inappropriate for ultrastructural localization (Mukherjee et al., 1998). Fluorescent compounds can also have photodynamic effects on $GABA_A$ receptors, independent of direct binding to the receptor (Eisenman et al., 2007; Shu et al., 2009). Thus, we sought an approach utilizing more modest chemical modification that would allow examination of preserved specimens. Combined photolabeling and click chemistry have been employed as powerful proteomic and biochemical tools (Lapinsky, 2012), but cell biological applications are only now emerging (Hofmann et al., 2014; Lapinsky, 2012; Peyrot et al., 2014). In recent cyto-localization studies, clickable analogues of cholesterol accumulated broadly in plasma-membrane and organelle compartments overlapping those that label with the fluorescent free-cholesterol marker filipin (Hofmann et al., 2014; Jao et al., 2015). By contrast, a clickable analogue of an oxidation product of cholesterol, 20(*S*)-hydroxycholesterol, compartmentalized selectively in Golgi through a mechanism dependent on lysosomal function and ATP (Peyrot et al., 2014). Here we exploit tandem *in situ* photolabeling and click chemistry to examine cell biological targets of drug-like analogues of neurosteroids, using an analogue that retains neurosteroid-like activity at $GABA_A$ receptors.

We used the novel GABA-active analogue and a set of inactive analogues to explore chemical requirements of neurosteroid-like accumulation and to explore the spatial impact on neuronal inhibition. We demonstrate that the active analogue compartmentalizes selectively in neuronal Golgi, a distribution distinct from cholesterol and not shared by some GABA-inactive analogues. On the other hand, Golgi-selective compartmentalization was not enantioselective and did not require energy, in contrast to other recent studies of similar molecules. We demonstrate that the soma-selective accumulation alters steroid actions relative to effects on dendrites and excised membrane patches, altering the steady-state effect of steroids the time course of effects.

2. MATERIALS AND METHODS

2.1 Cell culture

Animal use protocols were approved by the Washington University Animal Studies committee and procedures were consistent with the NIH guide for the care and use of Laboratory animals. All efforts were made to minimize animal use and suffering. Mixed hippocampal neuron/astrocyte cultures were prepared from postnatal day 1–3 rat pups of both sexes anesthetized with isoflurane, under protocols consistent with NIH guidelines and approved by the Washington University Animal Studies Committee. Methods were adapted from earlier descriptions (Huettner and Baughman, 1986; Mennerick et al., 1995). Hippocampal slices (500 μm thickness) were digested with 1 mg ml^{-1} papain in oxygenated Leibovitz L-15 medium (Life Technologies, Gaithersburg, MD, USA). Tissue was mechanically triturated in modified Eagle's medium (Life Technologies) containing 5% horse serum, 5% fetal calf serum, 17 mM D-glucose, 400 μM glutamine, 50 U ml^{-1} penicillin and 50 μg ml^{-1} streptomycin. Cells were seeded in modified Eagle's medium at a density of ~650 cells mm^{-2} onto 25 mm cover glasses coated with 5 mg ml^{-1} collagen or

with 0.1 mg ml^{-1} poly-D-lysine with 1 mg ml^{-1} laminin. Cultures were incubated at 37° C in a humidified ch amber with 5%CO_2/95% air. Cytosine arabinoside (6.7 μM) was added 3–4 days after plating to inhibit glial proliferation. The following day, half of the culture medium was replaced with Neurobasal medium plus B27 supplement (Life Technologies).

3T3 mouse embryonic fibroblast cells were seeded into 35-mm dishes and maintained in Dulbecco's modified Eagle's medium supplemented with 2 mM L-glutamine, 100 units/ml penicillin and streptomycin, and 10% fetal bovine serum at 37°C in a humidified atmosphere containing 5% CO_2. All media and chemicals used in the cell culture were obtained from Life Technologies.

2.2. *Xenopus* oocytes

Stage V–VI oocytes were removed from sexually mature female *Xenopus laevis* (*Xenopus* One) under 0.1% tricaine (3-aminobenzoic acid ethyl ester) anesthesia. Oocytes were defolliculated by shaking for 20 min at 37°C in collagenase (2 mg/ml) dissolved in calcium-free solution containing the following (in mM): NaCl (96), KCl (2), $MgCl_2$ (1), and HEPES (5) at pH 7.4.

Oocytes were used for initial screening as a source of a homogenous receptor population and to allow ready comparison to numerous other steroid analouges we have previously evaluated (e.g. Qian et al., 2014). Capped mRNA, encoding rat $GABA_A$ receptor α1, β2, γ2L subunits were transcribed *in vitro* using the mMESSAGE mMachine Kit (Ambion, Austin, TX, USA) from linearized pcDNA3 vectors containing receptor-coding regions. Subunit transcripts were injected in equal parts (3–13 ng RNA for each of the free α1, β2, γ2L subunits). *Xenopus* oocytes were recorded using standard two-electrode voltage-clamp recordings after incubation for up to 5 days at 18°C in ND96 medium containing (in mM): NaC l (96), KCl (1), $MgCl_2$ (1), $CaCl_2$ (2) and HEPES (10) at pH 7.4, supplemented with pyruvate (5 mM), penicillin (100 U ml^{-1}), streptomycin (100 μg ml^{-1}) and gentamycin (50 μg ml^{-1}).

2.3. Electrophysiology

Whole-cell patch clamp recordings were performed from hippocampal neurons in a saline solution containing (in mM) NaCl (138), KCl (4), $CaCl_2$ (2), $MgCl_2$ (1), glucose (10), HEPES (10), pH 7.25 with NaOH. Patch pipettes were filled with cesium methanesulfonate NaCl (130), $CaCl_2$ (0.5), EGTA (5), and HEPES (10) at pH 7.25, adjusted with KOH. For whole-cell recordings patch pipette resistances were 3–6 MΩ. Uncaging was performed with a shuttered metal halide light source and a standard fluorescein epifluorescence filter set. Uncaging at dendritic locations was performed at a fixed distance of 50–75 μm from the soma. To determine adequacy of clamp at dendritic sites of receptor activation, we examined reversal potential of somatic versus dendritic uncaged GABA responses in CsCl-filled cells. Reversal potentials of GABA responses at the two sites were indistinguishable (+1.9 ± 1.0 mV somatic vs. + 2.6 ± 0.6; n = 5 cells each, p = 0.58), suggesting reasonable voltage clamp and cytoplasmic perfusion of dendritic locations. Excised, outside-out patch recordings were performed with pipettes of 5–12 MΩ resistance filled with either CsCl or Cs methanesulfonate.

For oocyte recording, cells were transferred to a chamber containing unsupplemented ND96. Two-electrode voltage-clamp experiments were performed with an OC725 amplifier (Warner Instruments) 2–5 d after RNA injection. Intracellular recording pipettes were filled with 3 M KCl and had open tip resistances of ~1 MΩ. GABA and modulators were applied from a common tip of a gravity-driven multibarrel delivery system. Except when indicated, cells were voltage clamped at −70 mV, and the peak current or the current at the end of 30 s was measured as indicated.

2.4. Drugs and reagents

Suppliers for chemicals other than the novel steroids used were as follows: standard reagents and salts (Sigma-Aldrich), Rubi-GABA trimethylphospine (Tocris), DS2 (Tocris), and TO-PRO-3 (Life Technologies). Antibody species and sources were as follows: giantin (Covance Research Products Inc catalog PRB-114C-200, RRID:AB_10063713), PDI (Abcam catalog ab2792, RRID:AB_303304), COXIV (Abcam catalog ab16056, RRID:AB_443304) LAMP1 (rabbit, Millipore catalog CD107a, RRID:AB_10807184), NeuN (mouse; Millipore catalog MAB377, RRID:AB_2298772), GFAP (mouse, Boeringer Mannheim catalog 814-369, RRID:AB_2314534).

2.5. Steroids

The steroids were prepared by multistep synthetic procedures that are described in the Supplementary Materials. Spectroscopic data for all steroids are in the Supplemental material.

2.6. *In situ* click chemistry and immunostaining (culture and slices)

Cell cultures were incubated with 1 μM KK-123 for 15 min in saline containing (in mM): NaCl (138), KCl (4), $CaCl_2$ (2), $MgCl_2$ (1), glucose (10), HEPES (10), pH 7.25 with NaOH, 1 μM 2,3-dihydroxy-6-nitro-7-sulfamoyl-benzo[*f*]quinoxaline-2,3-dione (NBQX) and 50 μM D-(-)-2-Amino-5-phosphonopentanoic acid (D-APV). Cells were exposed to 365 nm light using a 0.15 A Blak-Ray lamp for 15 min at a distance of 2 cm. Afterward, cells were immediately fixed for click processing, immunocytochemistry, or filipin staining with 4% paraformaldehyde plus 0–0.02% glutaraldehyde in phosphate buffered saline (PBS) at room temperature for 10 minutes. For immunocytochemistry, cells were washed with PBS, incubated in 4% normal goat serum, and permeabilized with 0.05–0.1% Triton X-100. Cells were incubated in primary antibodies against anti-PDI, giantin, or COX IV for 2 h, followed by labeled secondary antibody (AlexaFluor 647, 1:500) for 1 h. For filipin staining, cells were incubated with filipin (50 μg/ml) in PBS for 1 h. After washing with PBS, the click reaction was performed by incubating fixed cells in 1 μM azide-488, a click reagent for fluorescence visualization (Click Chemistry Tools), in 100 μM Tris[(1-benzyl-1*H*-1,2,3-triazol-4-yl)methyl]amine, 2 mM ascorbic acid,1 mM $CuSO_4$ for 1 h in the dark, followed by three washes with PBS. For plasma membrane visualization, cells were incubated in CellMask Orange (ThermoFisher, 1 μM) before fixation.

In some experiments, cells were fixed prior to photo-attachment of KK-123 with 4% paraformaldehyde plus 0.02% glutaraldehyde in PBS at room temperature for 10 minutes. Cells were subsequently washed with PBS, incubated with 1 μM KK-123 in PBS for 15 min,

illuminated with the ultraviolet (UV) lamp for additional 15 min, then washed with PBS. Cells were permeabilized with 0.1% Triton X-100, then immunostained and clicked as above.

For chloroquine experiments, live hippocampal neurons or fibroblasts (NIH3T3 cells) were treated with 100 μM chloroquine or saline (controls) in their respective culture media for 30 min in a 37°C incubator. KK-123 (1 μM) was added for an other 15 min, followed by 365 nm illumination for 20 min, then immediately fixed with 4% paraformaldehyde plus 0.02% glutaraldehyde for 10 min. Cells were washed with PBS, and permeabilized with 4% normal goat serum and 0.1% Triton X-100 for 10 min. The click reaction was performed as above.

For tissue labeling, coronal slices from P20–P40 rat hippocampus were prepared with a Leica 1200S tissue slicer in low-sodium, sucrose buffer containing (in mM): NaCl (87), sucrose (75), $NaHCO_3$ (25), NaH_2PO_4 (1.25), KCl (2.5), $CaCl_2$ (0.5), $MgCl_2$ (3), and glucose (25), bubbled with carbogen. Slices were stored for 30 min at 34°C in a low-sodium choline solution that contained (in mM): choline chloride (92), KCl (2.5), $NaHCO_3$ (30), NaH_2PO_4 (1.25), $CaCl_2$ (2), $MgCl_2$ (1), glucose (25), HEPES (20), sodium ascorbate (5), thiourea (2), and sodium pyruvate (3); slices were then transferred to oxygenated solution of the above composition except that choline was omitted and NaCl was increased to 125 mM. Slices were incubated with 1 μM KK-123 for 15 min at room temperature in the presence of 1 μM (NBQX) and 50 μM D-APV, followed by illumination with 365 nm UV light for another 30 min. We did not assess whether steroid had reached a steady-state following the 45 min perfusion of slices. However, neurosteroid effects in previous work have reached a steady-state within ~10 min (Brown et al., 2015; Stell et al., 2003), and superficial cells with best access to perfused compounds were targeted for subsequent imaging. Tissue was immediately fixed with 4% paraformaldehyde plus 0.02% glutaraldehyde in PBS for 20 min. The click reaction as described above was performed overnight. Slices were then processed for immunostaining. Permeabilized tissue was then incubated in primary antibodies against anti-NeuN (1:3000) and GFAP (1:1000) or giantin (1:2000) overnight, followed by secondary antibodies and a nuclear stain (TO-PRO-3; 1:2000) for 2 h. Slices were coverslipped with Fluoromount-G.

Quantitation of click labeling and of immunostaining was performed using Metamorph (Molecular Devices) and the Fiji distribution of ImageJ imaging software (http://fiji.sc/Fiji).

2.7. Electron microscopy

Cell cultures were incubated with 1 μM KK-123, illuminated as above for 30 min, fixed with 4% paraformaldehyde plus 0.02% glutaraldehyde for 10 min, washed with PBS, then permeabilized with 0.02% Triton X-100 for 15 min. The click reaction was performed with 10 μM azide-biotin (Click Chemistry Tools) in 100 μM Tris[(1-benzyl-1H-1,2,3-triazol-4-yl)methyl]amine, 2 mM ascorbic acid,1 mM $CuSO_4$. The reaction was performed overnight in the dark, washed with PBS, incubated with streptavidin-HRP (1:500) for 2 h, incubated with diaminobenzidine (1:10, Vector Labs) for 60 s, and washed extensively with PBS. Cultures were fixed again in 1% paraformaldehyde and 4% glutaraldehyde in PBS for 20 min. at pH 7.4, washed, then incubated in 1% OsO_4 for 30 min, followed by 0.8% potassium ferricyanide for 30 min at room temperature. After rinsing with distilled water, specimens

were stained with 2% aqueous uranyl acetate for 30 min, dehydrated in ethanol, and embedded in poly/bed 812 for 24 h at 60° C. Sections were cut a t 50–70 nm and post-stained with uranyl acetate. Cells were photographed at 25,000x on a JEOL 100CX electron microscope with an AMT digital camera.

2.8. Statistics

Pooled data presented in the text and figures represent mean ± standard error of the mean. Comparisons between experimental and control mean values were made with repeated measures ANOVA in Figure 8 and paired and unpaired Student's t tests elsewhere. When multiple comparisons were made, a Bonferroni correction was performed. Significant differences were taken as $p < 0.05$.

3. RESULTS

3.1. KK-123 localization in Golgi

To localize cellular distribution of neuroactive steroids, we synthesized KK-123, a steroid analogue that retained GABA-modulator function and also contained functional groups for photolabeling and click chemistry visualization. KK-123 has structural features expected to promote activity at $GABA_A$ receptors. These features include a hydrogen bond donor at carbon 3 and hydrogen bond accepting group at the carbon 17 side chain. The analogue contains an alkyne group at carbon 2 for bio-orthogonal Cu(I)-catalyzed alkyne-azide cycloaddition (Hou et al., 2012) and a diazirine group at carbon 6 for carbene-mediated photo-attachment to proteins and hydrocarbons in the presence of 365 nm light (Dubinsky et al., 2012)(Figure 1A). KK-123 showed strong potentiation of GABA responses in hippocampal neurons at micromolar concentrations, consistent with actions of other neurosteroid analogues (Figure 1B)(Harrison et al., 1987).

We next attempted *in situ* visualization of the analogue using tandem photolabeling and click chemistry in cultured hippocampal neurons. Because diazirine photochemistry promotes both lipid and protein labeling (Chen et al., 2012a; Chen et al., 2012b), we expected to comprehensively and permanently label specific (e.g., $GABA_AR$) and non-specific (e.g., membranous) steroid-associated cellular pools in neurons and other cells. We incubated cells with 1 μM KK-123 with or without UV light exposure, followed by aldehyde cell fixation. We then used azide conjugated Alexa Fluor 488 for click-mediated fluorescence visualization. Figure 1C shows that labeling of hippocampal neurons in culture required the presence of KK-123 and UV light exposure, confirming the effectiveness of *in situ* photolabeling and the *in situ* click reaction.

The pattern of accumulation was mainly somatic with little neuritic labeling by KK-123, in general agreement with previous observations using fluorescent neurosteroid analogues (Akk et al., 2005). The compartmentalization of KK-123 seemed to parallel that of the Golgi network in neurons. This impression was confirmed in co-labeling studies in which we performed tandem photolabeling, click chemistry, and immunolabeling for the Golgi resident protein giantin (Figure 1D). To verify light microscopy results, we used azide-conjugated biotin to tag neurosteroid and streptavidin horseradish peroxidase/

diaminobenzidine to produce an electron-dense reaction product for electron microscopic evaluation. The reaction product marking KK-123 was located most prominently in Golgi and Golgi-associated structures (Figure 1E). Alternative organelle markers of PDI for endoplasmic reticulum (Figure 1F), COXIV for mitochondria (Figure 1G), and LAMP1 for lysosomes (not shown) failed to demonstrate selective co-localization. We note that we cannot exclude the possibility that Golgi outposts found in dendrites (Quassollo et al., 2015) harbored low levels of giantin and undetected steroid analogue in these studies. Control experiments that omitted UV exposure showed that gross neuronal morphology and the distribution of Golgi were not detectably altered by the UV exposure used for photolabeling (Supplementary Figure 1).

Cholesterol content has been proposed to be important for neurosteroid effects on $GABA_A$ receptors (Sooksawate and Simmonds, 1998). To test whether KK-123 accumulated in cholesterol rich sites, we co-labeled cells with the fluorescent marker of free cholesterol, filipin (Figure 1H). Although partial overlap was evident, particularly in somatic regions (Figure 1H, right), filipin labeling was enriched in the plasma membrane whereas KK-123 accumulation was detectable but not enriched. This led to a profile of labeling in which filipin was more evident in distal neurites than KK-123. Furthermore, in some studies we used CellMask Orange to label plasma membrane (Boudes et al., 2009; Hirota et al., 2010; Sheldahl et al., 2008). KK-123 fluorescence in single confocal planes was evaluated through a line that traversed the plasma membrane and the intracellular compartment. The intracellular KK-123 fluorescence was 4.6 ± 1.5-fold higher than KK-123 fluorescence intensity at the peak of the plasma-membrane labeling (Supplementary Figure 2). Thus, taken together, results with a clickable neurosteroid photolabel show Golgi-selective partitioning, leading to strong somatic accumulation and less KK-123 in neuronal processes and on the cell surface.

The hippocampal cultures employed contain neurons resting on a bed of astrocytes, but we noticed little KK-123 accumulation in astrocytes. To determine whether this was the result of qualitative or quantitative differences, we performed *in situ* labeling in acutely prepared hippocampal slices (Figure 2), where astrocyte and neuronal morphology is better preserved than in dissociated cultures. We found that although astrocyte KK-123 labeling was weaker than neuronal labeling (Figure 2A, B), this likely reflects less Golgi membrane in astrocytes, since giantin labeling in astrocytes was also weaker than in neurons (Figure 2C,D). We conclude that neuron-selective compartmentalization of KK-123 is likely a secondary by-product of Golgi-selective accumulation.

3.2. Impact of chemical structure on Golgi-selective accumulation

Perhaps the Golgi network represents the majority of neuronal intracellular membrane, and the observed selective compartmentalization is through passive, non-specific lipophilic interactions with membranes. If so, we would expect other neurosteroid-like clickable photolabels with similar or greater lipophilicity to exhibit an accumulation pattern similar to that of KK-123. We prepared several steroid analogues with varying structures (Figure 3A). All analogues exhibited much weaker activity than KK-123 at $GABA_A$ receptors (Figure 3B,C, F), but all compounds robustly labeled intracellular compartments. We examined co-

localization with Golgi by computing the correlation coefficient between giantin labeling and compound labeling along a line drawn through the soma of individual neurons in individual confocal planes (Figure 3D, E). Giantin labeling, without regard for analogue labeling, was used to define the line trajectory, and the line was chosen to highlight variability in labeling. KK-150 contained the diazirine photolabel in place of the 3α-OH group and harbored the alkyne tag in a 17α configuration. These structural changes also resulted in stronger estimated lipophilicity compared with KK-123 (logP 6.12 vs. 4.45). In addition to its absent activity at $GABA_A$ receptors, KK-150 exhibited a dramatically different pattern of cellular accumulation, largely avoiding Golgi (Figure 3E, G). Interestingly, labeling by KK-150 was much less UV dependent, compared with KK-123 labeling; strong accumulation and retention of KK-150 was observed even in the absence of UV illumination (data not shown). We hypothesize that strong photolabel-independent accumulation may arise from strong lipophilicity. However, we conclude that liphophilicity alone cannot explain Golgi-selective accumulation of KK-123.

Although KK-150 had no detectable activity at $GABA_A$ receptors, analysis of other analogues showed that activity at $GABA_A$ receptors is not required for Golgi accumulation. This was evident most dramatically in the enantiomer of KK-123, KK-152 (Figure 3A). Enantioselective interactions are taken as a hallmark of specific ligand-protein interactions, resulting in part from the composition of proteins exclusively of L-amino acid residues. For instance, as expected, KK-152 showed no potentiating activity at $GABA_A$ receptors at concentrations up to 10 μM (Figure 3F), consistent with a direct receptor interaction of KK-123 (Covey, 2008). On the other hand, reversing all chiral centers of KK-123 failed to alter the Golgi-selective pattern of accumulation relative to KK-123 (Figure 3G). The indistinguishable compartmentalization of KK-152 relative to KK-123 is consistent with the idea that ligand-protein interactions do not contribute strongly to the accumulation pattern and supports previous observations showing that enantiomers behave indistinguishably in model membranes (Alakoskela et al., 2007). Although a failure to find enantioselectivity for KK-123 localization in the Golgi cannot exclude the possibility that a protein binds KK-123 non-enantioselectivity, we consider this possibility unlikely and unnecessary to explain the results.

Several other GABA-inactive analogues exhibited Golgi selectivity intermediate to that of KK-123/KK-152 on the one hand and KK-150 on the other (Figure 3G). KK-139, KK-148, and MQ-127 (Figure 3A) showed various structural variations from KK-123, and each exhibited significantly less Golgi selectivity compared with KK-123 (Figure 3G). Interestingly, a change in stereochemistry of the hydroxyl group at carbon 3 was sufficient to reduce Golgi selective accumulation (Figure 3G, KK-123 vs. KK-139), despite identical calculated logP values of the two compounds. Similarly, KK-150 and KK-148, which also have high, identical predicted logP values, differed only in the stereochemistry of the alkyne chain configuration at carbon 17, and demonstrated significantly different degrees of Golgi co-localization ($p < 0.05$, Bonferroni corrected t-test).

It should be noted that experimental logP values for compounds with the same calculated logP values may differ slightly, but calculated logP values are generally accepted as providing a good estimate of experimental logP values. For instance, although epimers (e.g.,

KK-148 and KK-150) and regioisomers (KK-123 and MQ-127) may have different measured logP values (Testa et al., 2008), any logP differences within such pairs will be small relative to those caused by structural changes such as removal or addition of a hydroxyl group. Taken together, the results in Figure 3G, indicate that although logP is unlikely to dictate Golgi localization, stereochemical differences in structure clearly affect Golgi localization. It may well be the case that different steroids reside selectively in membranes of different composition in various cellular organelles. This would not be surprising because even cholesterol is not uniformly distributed in cellular membranes (Gimpl and Gehrig-Burger, 2007; Hofmann et al., 2014; Mukherjee et al., 1998).

3.3. Energy dependence of KK-123 accumulation

To gain additional insight into factors that influence selective accumulation of KK-123 in Golgi membranes, we determined if this localization was energy dependent in neurons and in 3T3 fibroblasts. Previously, it was shown that 20(*S*)-hydroxycholesterol exhibits Golgi-selective accumulation in 3T3 fibroblast cells through a lysosome-dependent, active mechanism (Peyrot et al., 2014). This pathway presumably involves endocytosis from the plasma membrane, followed by trafficking through late endosomes and lysosomes, eventually to the Golgi; in addition to accounting for compartmentalization of the oxysterol 20(S)-hydroxycholesterol, this pathway appears to account for Golgi accumulation of glycophospholipids (Marks and Pagano, 2002). We first challenged 3T3 cells with KK-123 to determine whether KK-123 accumulation in this cell type obeys a similar mechanism to the previously examined oxysterol. Co-labeling with giantin revealed strong co-localization (data not shown), as with neurons. Because 3T3 cells do not express $GABA_A$ receptors, this result also excludes an important role for intracellular, Golgi-resident $GABA_A$ receptors as a target of KK-123 accumulation. When we inhibited lysosomal function in 3T3 cells with chloroquine, KK-123 labeling was decreased (Figure 4A,B), a result essentially similar to that obtained with the analogue of 20(*S*)-hydroxycholesterol in this cell type (Peyrot et al., 2014). In contrast, inhibition of lysosomal function with chloroquine failed to dampen KK-123 labeling in neurons (Figure 4C,D). In fact, labeling was slightly but significantly increased (Figure 4D). We conclude that KK-123 in neurons is not dependent on lysosomal function and that compartmentalization mechanisms can differ by cell type even when patterns of compartmentalization appear superficially similar.

To address energy dependence, we reasoned that we could address the entire complement of ATP dependent mechanisms of compartmentalization by comparing live cells with fixed neurons, which can no longer utilize metabolic pathways. We thus compared KK-123 labeling in aldehyde-fixed cells versus live cells. To our surprise, we found that cells that were fixed before KK-123 incubation exhibited altered intensity of labeling but no alteration in the selective, Golgi-preferred pattern of accumulation (Figure 5). Overall, in experiments analyzed with a correlation analysis similar to that depicted in Figure 3D,E, the average correlation coefficient between linescans of KK-123 and giantin labeling in fixed cells was 0.69 ± 0.03, no different than cohort-matched live cells 0.65 ± .03 ($p = 0.43$ in 20 cells from 6 experiments). The slightly reduced intensity of labeling by KK-123 in fixed cells (Figure 5B) did not necessarily reflect an energy dependent component of compartmentalization since a different fixative (2% glutaraldehyde) resulted in brighter KK-123 labeling of fixed

cells than live cells, still exhibiting a heavily Golgi-selective pattern (data not shown). We conclude that metabolic viability is not required for Golgi-selective accumulation and that energy-dependent mechanisms do not need to be invoked to explain the Golgi-selective compartmentalization.

3.4. Functional impact of Golgi-selective compartmentalization on inhibition

What is the functional impact of Golgi-selective partitioning on GABA-mediated inhibition, the main known target of the neurosteroid class examined here? We reasoned that because of the large capacity of the intracellular reservoir, accumulation in somatic Golgi will reduce the amount of steroid available to plasma-membrane GABA receptors on or near the soma. By contrast dendrites would experience relatively little “Golgi shunt.” First, we established that whole-cell recording itself does not dramatically alter steroid accumulation. Using a previously characterized fluorescent, GABA-active steroid (Akk et al., 2005), we compared intact cells with whole cells and found no difference in time course of somatic accumulation (Supplemental Figure 3). We evaluated somatic/dendritic differences using caged GABA photolyzed either on the soma or on a dendrite during continuous bath presence of KK-123. The experimental setup is schematized in Figure 6A,B. GABA was released by a 488 nm fluorescent light constrained to either the soma (circle in Figure 6A) or to a dendrite (circle in figure 6B). As shown in Figure 6C,D, KK-123 (0.1 μM) potentiated GABA responses elicited from dendrites significantly more than GABA responses elicited from the soma.

It is possible that receptor subunit composition dictates the dendritic superiority. Specifically, δ subunit-containing $GABA_A$ receptors are more sensitive to neurosteroids than non-δ counterparts (Wohlfarth et al., 2002). To test this possibility, we used the δ-selective positive allosteric modulator DS2 (Wafford et al., 2009) in place of KK-123 in the same experimental paradigm. We found no spatial selectivity of 1 μM DS2 potentiation (Figure 6F), indicating that δ subunit containing receptors are not differentially distributed on dendrites vs. somas.

To test the alternative explanation that a systematic difference in GABA concentration was achieved during soma uncaging vs. dendrite uncaging, we exploited the agonist concentration dependence of potentiation. Positive allosteric modulation is sensitive to GABA concentration, with low concentrations of agonist more sensitive to potentiation. Although the DS2 result suggests that this is unlikely, to test more definitively this alternative explanation, we employed pentobarbital (20 μM), which is mechanistically similar to neurosteroids (Steinbach and Akk, 2001) but for which intracellular accumulation is not expected to be prominent (Shu et al., 2004). Figure 6G shows that pentobarbital had no spatially selective effect on inhibition. Taken together, the results suggest that somatic accumulation lowers the effective steroid concentration, reducing the impact on proximal inhibition compared with distal inhibition, where accumulation contributes less.

To further test the possibility that different receptor subunits were responsible for the different steroid sensitivity, we excised patches from soma or from dendrites at locations approximating uncaging locations (50–75 μm from the soma). We challenged patches with 1 μM GABA and 100 nM KK-123 (Figure 6H,I). Excised outside-out patches from somas and dendrites showed no difference in KK-123 potentiation (Figure 6H–J). This result supports

the idea that receptor differences cannot explain the different sensitivity of somas versus dendrites.

If the soma contains a steroid reservoir, we would also expect the reservoir to influence whole-cell but not excised-patch responsiveness to steroid application. Indeed, peak potentiation by both KK-123 (2 μM) and 3α5αP (1 μM) was stronger in excised patches from somas than in whole-cell somatic recordings exposed to GABA (Figure 7). Whole-cell potentiation rose more slowly than that of patches and showed little desensitization. Patch currents showed a rapid desensitization in the presence of steroid, as if receptors were operating at a high open probability with saturating steroid concentration (Figure 7A,D). Whole-cell potentiation also exhibited incomplete removal by the membrane-impermeant steroid scavenger γ-cyclodextrin (500 μM)(Shu et al., 2004; Shu et al., 2007) applied for 3 s, suggesting a reservoir in whole-cell recordings, but not in excised patches, that supplies receptors (Figure 7B,E). Although the same perfusion apparatus was used for both patches and whole-cell recordings, perfusion of whole cells was undoubtedly slower than perfusion of small excised membrane patches. However, the differences between patches and whole cells cannot be explained by the perfusion rate difference because Mg^{2+} (10 μM) block of whole-cell NMDA currents showed a 62 ± 9 ms onset time constant and 228 ± 56 ms offset time constant, well below the 3 s application time of γ-cyclodextrin (Supplemental Figure 4).

A somatic siphoning action also predicts that the time course of effects following removal of aqueous steroid may be faster at the soma than at the dendrites. We tested this idea using repetitive GABA uncaging on somas and dendrites in the presence of neurosteroid. We first pre-applied steroid to potentiate the GABA response, then removed steroid by bath perfusion while monitoring potentiation using GABA uncaging (Figure 8). For KK-123 (100 nM), steroid wash out was extremely slow from both soma and dendrites, possibly reflecting the strong hydrophobicity of the compound, and we were unable to detect a difference in loss of steroid from the two compartments (Supplementary Figure 5). However, for the less hydrophobic, endogenous compound 3α5αP (50 nM), the effects of steroid on somatic GABA responses returned to baseline faster than dendritic responses during saline wash, consistent with the hypothesis that the somatic compartment contains an additional route of escape for proximal plasma-membrane steroid (Figure 8C). We reasoned that we may be able to change the intracellular Golgi reservoir from a net sink into a net source by rapidly removing free exterior steroid with γ-cyclodextrin. With cyclodextrin wash, the dendritic pool was more readily extracted than the somatic pool (Figure 8C), consistent with a somatic reserve inaccessible to the cell impermeant scavenger and revealed by the absence of continued influx into the reservoir. In summary, these results are consistent with the idea that the soma-selective accumulation of steroid observed in Figures 1–5 reduces the effect of steroid on proximal inhibition relative to distal inhibition.

4. DISCUSSION

Here we studied the impact of compartmental accumulation of neurosteroid on $GABA_A$ receptor modulation. To do so, we synthesized a neurosteroid analogue with $GABA_A$ receptor enhancing activity, photolability, and clickability. This allowed us to permanently

tag sites of accumulation *in situ* by photolabeling, followed by bio-orthogonal click chemistry to visualize accumulation with azide-conjugated markers. To our knowledge, our work is the first to demonstrate a differential effect of neurosteroids on distal vs. proximal inhibition, and we link this differential effect to specific but passive accumulation at the sub-cellular level.

Several modes of accumulation and retention appear evident from past work and the present work. Our studies made use of *in situ* photolabeling to identify cellular neurosteroid at high resolution. Other recent similar approaches examining other cellular signaling molecules did not appear to require a photolabeling strategy for click cyto-localization (Jao et al., 2015; Peyrot et al., 2014; Viertler et al., 2012). In those cases, non-covalent cyto-localization likely occurs because the molecules have high-affinity protein interactions. This is not the case for neurosteroids acting at plasma-membrane $GABA_A$ receptors. Neurosteroids are unlikely to bind with high affinity to these targets but require high local plasma-membrane concentration for receptor modulation (Chisari et al., 2010; Chisari et al., 2009). Despite the presumed high membrane concentration of KK-123, intracellular compartmentalization in Golgi membranes dwarfs any plasma membrane signal, even with the aid of photolabeling to retain steroid. Finally, the analogue KK-150, which is even more lipophilic than KK-123, is retained in cells without UV exposure. Because any targets for KK-150 are unknown, it remains unclear whether retention is through high-affinity interactions with proteins or because of lipophilic interactions resulting in part from the high lipophilicity of this compound.

Our strategy assumes that photolabeling efficiency is similar in all compartments. For instance, is weak labeling of plasma membrane by KK-123 a result of poor photolabeling in this compartment? Although we cannot definitively answer this question, past studies examining the accumulation of fluorescent neurosteroid analogues also failed to strongly label plasma membrane (Akk et al., 2005), and the pattern of accumulation with these previous analogues is strongly reminiscent of that observed with the click photolabel.

Our results argue for an energy independent, protein independent mechanism of KK-123 accumulation. Cell viability and functional lysosomes were not required for Golgi-selective accumulation (Figures 4,5), and accumulation was not enantioselective (Figure 3). This is in contrast to Golgi-selective accumulation of an oxysterol which exhibits a lysosome dependent and energy dependent Golgi-selective accumulation that is enantioselective (Peyrot et al., 2014). Because Golgi-selective accumulation was not evident with all the lipophilic, steroid analogues, Golgi-selective accumulation appears to require specific structural attributes of the compounds (Figure 3). This is consistent with earlier findings that steroids in model membranes exhibit stereoselectivity (diastereoselectivity), but not enantioselectivity(Alakoskela et al., 2007).

One hypothesis to explain the observed results is that the specific lipid composition of Golgi accounts for the selective association of some steroid analogues but not others with these organelles. The lipid composition of organelle membranes becomes increasingly asymmetric and enriched in sterols and sphingomyelin in the secretory pathway progression from endoplasmic reticulum through cis- and trans-Golgi to plasma membrane. A sterol-rich

membrane per se does not favor neurosteroid accumulation, because filipin labeling only partially overlapped that of KK-123 (Figure 1H). However, we hypothesize that the specific mixture of lipid components of the Golgi (Drin, 2014; van Meer and Sprong, 2004) is a determinant of the cellular distribution of neurosteroid analogues.

Regardless of precise mechanism of neurosteroid accumulation in the Golgi, we identified a previously unrecognized functional impact of the accumulation with a differential effect of neurosteroids on proximal vs. distal inhibition, which we attribute to a somatic intracellular reservoir of large capacity. Although we focused on the indirect effect of Golgi accumulation on plasma-membrane $GABA_A$ receptors, we cannot exclude the possibility that the Golgi-associated steroid is not inert and may have biological targets there. For instance, although Golgi compartmentalization of steroid was not dependent on Golgi-resident $GABA_A$Rs (Figure 4), steroids could have a chaperoning effect on Golgi $GABA_A$Rs and could alter surface expression of the receptors (Eshaq et al., 2010). There could also be novel targets of neurosteroids in the Golgi that affect Golgi function. Such effects await further study.

In examining the impact of Golgi-associated steroid on plasma-membrane $GABA_A$R function, our results favor somatic accumulation as an escape path for steroid from the plasma membrane, which lowers its effective concentration and speeds offset of actions at $GABA_A$ receptors. Figures 7 and 8C suggest that the intracellular reservoir might also act as a source under some conditions. This is also supported by previous experiments (Akk et al., 2005; Tokuda et al., 2010). By developing GABA-active neurosteroids with different accumulation properties, effects may be biased toward either distal or proximal GABA receptors. For instance, neurosteroids bind tubulin (Chen et al., 2012a). By engineering a steroid with enhanced microtubule interaction and reduced Golgi accumulation, steroid effects might be designed to favor the reverse selectivity (proximal over distal) of that observed in the present study. The practicality of this strategy awaits more information about the overlap between structure-activity at $GABA_A$ receptors and structural features governing cellular partitioning.

Finally, we consider the impact of the somatic reservoir on endogenous steroid compartmentalization and storage. All of our data were generated from exogenous application. However, other studies have demonstrated the impact of endogenously synthesized steroids (Belelli and Lambert, 2005). Depending on the source of synthesis (neurons versus glia, for instance), steroid accumulation in Golgi may differentially influence somatic inhibition, as we have observed. Golgi accumulation and retention could help observed regional, sub-regional, and autocrine localization of steroid effects in thalamus (Brown et al., 2015), spinal cord (Inquimbert et al., 2008) and hippocampus (Tokuda et al., 2010).

Supplementary Material

Refer to Web version on PubMed Central for supplementary material.

Acknowledgments

The authors thank members of the Taylor Family Institute for Innovative Psychiatric Research for discussion, Courtney Sobieski with help on initial co-labeling analysis, Ann Benz for technical help with cultures, and Dr. Nicholas Davidson for NIH3T3 cells. We gratefully acknowledge support from the Bantly Foundation and from National Institutes of Health National Institute on Alcohol Abuse and Alcoholism [Grant R01AA017413]; National Institute of General Medicine [Grants P01GM47969, R01GM108799]; and National Institute of Mental Health [Grants R01MH077791, R01MH078823, R01MH101874, and R21MH104506].

Abbreviations

Steroid analogues synthesized for the present work are referenced by non-standard abbreviations. Their chemical structures are supplied in the manuscript.

D-APV	D-(-)-2-Amino-5-phosphonopentanoic acid
DS2	4-Chloro-N-[2-(2-thienyl)imidazo[1,2-a]pyridin-3-yl]benzamide
NBQX	2,3-dihydroxy-6-nitro-7-sulfamoyl-benzo[f]quinoxaline-2,3-dione

References

Akk G, Shu HJ, Wang C, Steinbach JH, Zorumski CF, Covey DF, Mennerick S. Neurosteroid access to the $GABA_A$ receptor. Journal of Neuroscience. 2005; 25:11605–11613. [PubMed: 16354918]

Alakoskela JM, Covey DF, Kinnunen PK. Lack of enantiomeric specificity in the effects of anesthetic steroids on lipid bilayers. Biochim Biophys Acta. 2007; 1768:131–145. [PubMed: 16945324]

Antkowiak B. How do general anaesthetics work? Naturwissenschaften. 2001; 88:201–213. [PubMed: 11482433]

Belelli D, Herd MB, Mitchell EA, Peden DR, Vardy AW, Gentet L, Lambert JJ. Neuroactive steroids and inhibitory neurotransmission: mechanisms of action and physiological relevance. Neuroscience. 2006; 138:821–829. [PubMed: 16310966]

Belelli D, Lambert JJ. Neurosteroids: endogenous regulators of the $GABA_A$ receptor. Nat Rev Neurosci. 2005; 6:565–575. [PubMed: 15959466]

Boudes M, Sar C, Menigoz A, Hilaire C, Pequignot MO, Kozlenkov A, Marmorstein A, Carroll P, Valmier J, Scamps F. Best1 is a gene regulated by nerve injury and required for Ca2+-activated Cl- current expression in axotomized sensory neurons. Journal of Neuroscience. 2009; 29:10063–10071. [PubMed: 19675239]

Brown AR, Herd MB, Belelli D, Lambert JJ. Developmentally regulated neurosteroid synthesis enhances GABAergic neurotransmission in mouse thalamocortical neurones. J Physiol. 2015; 593:267–284. [PubMed: 25556800]

Chen ZW, Chen LH, Akentieva N, Lichti CF, Darbandi R, Hastings R, Covey DF, Reichert DE, Townsend RR, Evers AS. A neurosteroid analogue photolabeling reagent labels the colchicine-binding site on tubulin: a mass spectrometric analysis. Electrophoresis. 2012a; 33:666–674. [PubMed: 22451060]

Chen ZW, Manion B, Townsend RR, Reichert DE, Covey DF, Steinbach JH, Sieghart W, Fuchs K, Evers AS. Neurosteroid analog photolabeling of a site in the third transmembrane domain of the beta3 subunit of the GABA(A) receptor. Mol Pharmacol. 2012b; 82:408–419. [PubMed: 22648971]

Chisari M, Eisenman LN, Covey DF, Mennerick S, Zorumski CF. The sticky issue of neurosteroids and $GABA_A$ receptors. Trends Neurosci. 2010; 33:299–306. [PubMed: 20409596]

Chisari M, Eisenman LN, Krishnan K, Bandyopadhyaya AK, Wang C, Taylor A, Benz A, Covey DF, Zorumski CF, Mennerick S. The influence of neuroactive steroid lipophilicity on $GABA_A$ receptor modulation: evidence for a low-affinity interaction. Journal of Neurophysiology. 2009; 102:1254–1264. [PubMed: 19553485]

Covey DF. ent-Steroids: Novel tools for studies of signaling pathways. Steroids. 2008

Drin G. Topological regulation of lipid balance in cells. Annu Rev Biochem. 2014; 83:51–77. [PubMed: 24606148]

Dubinsky L, Krom BP, Meijler MM. Diazirine based photoaffinity labeling. Bioorg Med Chem. 2012; 20:554–570. [PubMed: 21778062]

Eisenman LN, Shu HJ, Akk G, Wang C, Manion BD, Kress GJ, Evers AS, Steinbach JH, Covey DF, Zorumski CF, Mennerick S. Anticonvulsant and anesthetic effects of a fluorescent neurosteroid analog activated by visible light. Nat Neurosci. 2007; 10:523–530. [PubMed: 17322875]

Eshaq RS, Stahl LD, Stone R 2nd, Smith SS, Robinson LC, Leidenheimer NJ. GABA acts as a ligand chaperone in the early secretory pathway to promote cell surface expression of GABAA receptors. Brain Res. 2010; 1346:1–13. [PubMed: 20580636]

Gimpl G, Gehrig-Burger K. Cholesterol reporter molecules. Biosci Rep. 2007; 27:335–358. [PubMed: 17668316]

Harrison NL, Majewska MD, Harrington JW, Barker JL. Structure-activity relationships for steroid interaction with the gamma-aminobutyric acidA receptor complex. Journal of Pharmacology and Experimental Therapeutics. 1987; 241:346–353. [PubMed: 3033209]

Hirota N, Yasuda D, Hashidate T, Yamamoto T, Yamaguchi S, Nagamune T, Nagase T, Shimizu T, Nakamura M. Amino acid residues critical for endoplasmic reticulum export and trafficking of platelet-activating factor receptor. J Biol Chem. 2010; 285:5931–5940. [PubMed: 20007715]

Hofmann K, Thiele C, Schött HF, Gaebler A, Schoene M, Kiver Y, Friedrichs S, Lütjohann D, Kuerschner L. A novel alkyne cholesterol to trace cellular cholesterol metabolism and localization. J Lipid Res. 2014; 55:583–591. [PubMed: 24334219]

Hou J, Liu X, Shen J, Zhao G, Wang PG. The impact of click chemistry in medicinal chemistry. Expert Opin Drug Discov. 2012; 7:489–501. [PubMed: 22607210]

Huettner JE, Baughman RW. Primary culture of identified neurons from the visual cortex of postnatal rats. Journal of Neuroscience. 1986; 6:3044–3060. [PubMed: 3760948]

Inquimbert P, Rodeau JL, Schlichter R. Regional differences in the decay kinetics of GABA(A) receptor-mediated miniature IPSCs in the dorsal horn of the rat spinal cord are determined by mitochondrial transport of cholesterol. Journal of Neuroscience. 2008; 28:3427–3437. [PubMed: 18367609]

Jao CY, Nedelcu D, Lopez LV, Samarakoon TN, Welti R, Salic A. Bioorthogonal probes for imaging sterols in cells. Chembiochem. 2015; 16:611–617. [PubMed: 25663046]

Lapinsky DJ. Tandem photoaffinity labeling-bioorthogonal conjugation in medicinal chemistry. Bioorg Med Chem. 2012; 20:6237–6247. [PubMed: 23026086]

Li P, Shu HJ, Wang C, Mennerick S, Zorumski CF, Covey DF, Steinbach JH, Akk G. Neurosteroid migration to intracellular compartments reduces steroid concentration in the membrane and diminishes GABA-A receptor potentiation. J Physiol. 2007; 584:789–800. [PubMed: 17761771]

Marks DL, Pagano RE. Endocytosis and sorting of glycosphingolipids in sphingolipid storage disease. Trends Cell Biol. 2002; 12:605–613. [PubMed: 12495850]

Mennerick S, Que J, Benz A, Zorumski CF. Passive and synaptic properties of hippocampal neurons grown in microcultures and in mass cultures. Journal of Neurophysiology. 1995; 73:320–332. [PubMed: 7714575]

Mukherjee S, Zha X, Tabas I, Maxfield FR. Cholesterol distribution in living cells: Fluorescence imaging using dehydroergosterol as a fluorescent cholesterol analog. Biophysical Journal. 1998; 75:1915–1925. [PubMed: 9746532]

Peyrot SM, Nachtergaele S, Luchetti G, Mydock-McGrane LK, Fujiwara H, Scherrer D, Jallouk A, Schlesinger PH, Ory DS, Covey DF, Rohatgi R. Tracking the subcellular fate of 20(s)-hydroxycholesterol with click chemistry reveals a transport pathway to the Golgi. J Biol Chem. 2014; 289:11095–11110. [PubMed: 24596093]

Qian M, Krishnan K, Kudova E, Li P, Manion BD, Taylor A, Elias G, Akk G, Evers AS, Zorumski CF, Mennerick S, Covey DF. Neurosteroid analogues. 18. Structure-activity studies of ent-steroid potentiators of gamma-aminobutyric acid type A receptors and comparison of their activities with those of alphaxalone and allopregnanolone. J Med Chem. 2014; 57:171–190. [PubMed: 24328079]

Quassollo G, Wojnacki J, Salas Daniela A, Gastaldi L, Marzolo María P, Conde C, Bisbal M, Couve A, Cáceres A. A RhoA Signaling Pathway Regulates Dendritic Golgi Outpost Formation. Current Biology. 2015; 25:971–982. [PubMed: 25802147]

Sheldahl LC, Shapiro RA, Bryant DN, Koerner IP, Dorsa DM. Estrogen induces rapid translocation of estrogen receptor beta, but not estrogen receptor alpha, to the neuronal plasma membrane. Neuroscience. 2008; 153:751–761. [PubMed: 18406537]

Shu HJ, Eisenman LN, Jinadasa D, Covey DF, Zorumski CF, Mennerick S. Slow actions of neuroactive steroids at $GABA_A$ receptors. Journal of Neuroscience. 2004; 24:6667–6675. [PubMed: 15282269]

Shu HJ, Eisenman LN, Wang C, Bandyopadhyaya AK, Krishnan K, Taylor A, Benz AM, Manion B, Evers AS, Covey DF, Zorumski CF, Mennerick S. Photodynamic effects of steroid-conjugated fluorophores on $GABA_A$ receptors. Mol Pharmacol. 2009; 76:754–765. [PubMed: 19596835]

Shu HJ, Zeng CM, Wang C, Covey DF, Zorumski CF, Mennerick S. Cyclodextrins sequester neuroactive steroids and differentiate mechanisms that rate limit steroid actions. Br J Pharmacol. 2007; 150:164–175. [PubMed: 17160009]

Sooksawate T, Simmonds MA. Increased membrane cholesterol reduces the potentiation of GABAA currents by neurosteroids in dissociated hippocampal neurones. Neuropharmacology. 1998; 37:1103–1110. [PubMed: 9833640]

Steinbach JH, Akk G. Modulation of $GABA_A$ receptor channel gating by pentobarbital. Journal of Physiology (London). 2001; 537:715–733. [PubMed: 11744750]

Stell BM, Brickley SG, Tang CY, Farrant M, Mody I. Neuroactive steroids reduce neuronal excitability by selectively enhancing tonic inhibition mediated by δ subunit-containing $GABA_A$ receptors. Proceedings of the National Academy of Sciences of the United States of America. 2003; 100:14439–14444. [PubMed: 14623958]

Testa, B.; Carrupt, PA.; Gaillard, P.; Tsai, RS. Lipophilicity in Drug Action and Toxicology. Wiley-VCH Verlag GmbH; 2008. Intramolecular Interactions Encoded in Lipophilicity: Their Nature and Significance; p. 49-71.

Tokuda K, O'Dell KA, Izumi Y, Zorumski CF. Midazolam inhibits hippocampal long-term potentiation and learning through dual central and peripheral benzodiazepine receptor activation and neurosteroidogenesis. Journal of Neuroscience. 2010; 30:16788–16795. [PubMed: 21159950]

van Meer G, Sprong H. Membrane lipids and vesicular traffic. Curr Opin Cell Biol. 2004; 16:373–378. [PubMed: 15261669]

Viertler M, Schittmayer M, Birner-Gruenberger R. Activity based subcellular resolution imaging of lipases. Bioorg Med Chem. 2012; 20:628–632. [PubMed: 21570307]

Wafford KA, van Niel MB, Ma QP, Horridge E, Herd MB, Peden DR, Belelli D, Lambert JJ. Novel compounds selectively enhance δ subunit containing $GABA_A$ receptors and increase tonic currents in thalamus. Neuropharmacology. 2009; 56:182–189. [PubMed: 18762200]

Wohlfarth KM, Bianchi MT, Macdonald RL. Enhanced neurosteroid potentiation of ternary $GABA_A$ receptors containing the δ subunit. Journal of Neuroscience. 2002; 22:1541–1549. [PubMed: 11880484]

Zorumski CF, Mennerick S, Isenberg KE, Covey DF. Potential clinical uses of neuroactive steroids. Curr Opin Investig Drugs. 2000; 1:360–369.

Zorumski CF, Paul SM, Izumi Y, Covey DF, Mennerick S. Neurosteroids, stress and depression: potential therapeutic opportunities. Neurosci Biobehav Rev. 2013; 37:109–122. [PubMed: 23085210]

Highlights

- Neurosteroids accumulate inside neurons, which may reduce their access to surface $GABA_A$ receptors.
- Neuroactive steroids accumulate preferentially in somatic Golgi.
- This selective Golgi compartmentalization does not depend directly or indirectly on ATP.
- Somatic Golgi compartmentalization results in weaker, more rapidly reversible effects at somatic $GABA_A$ receptors compared with dendritic $GABA_A$ receptors.

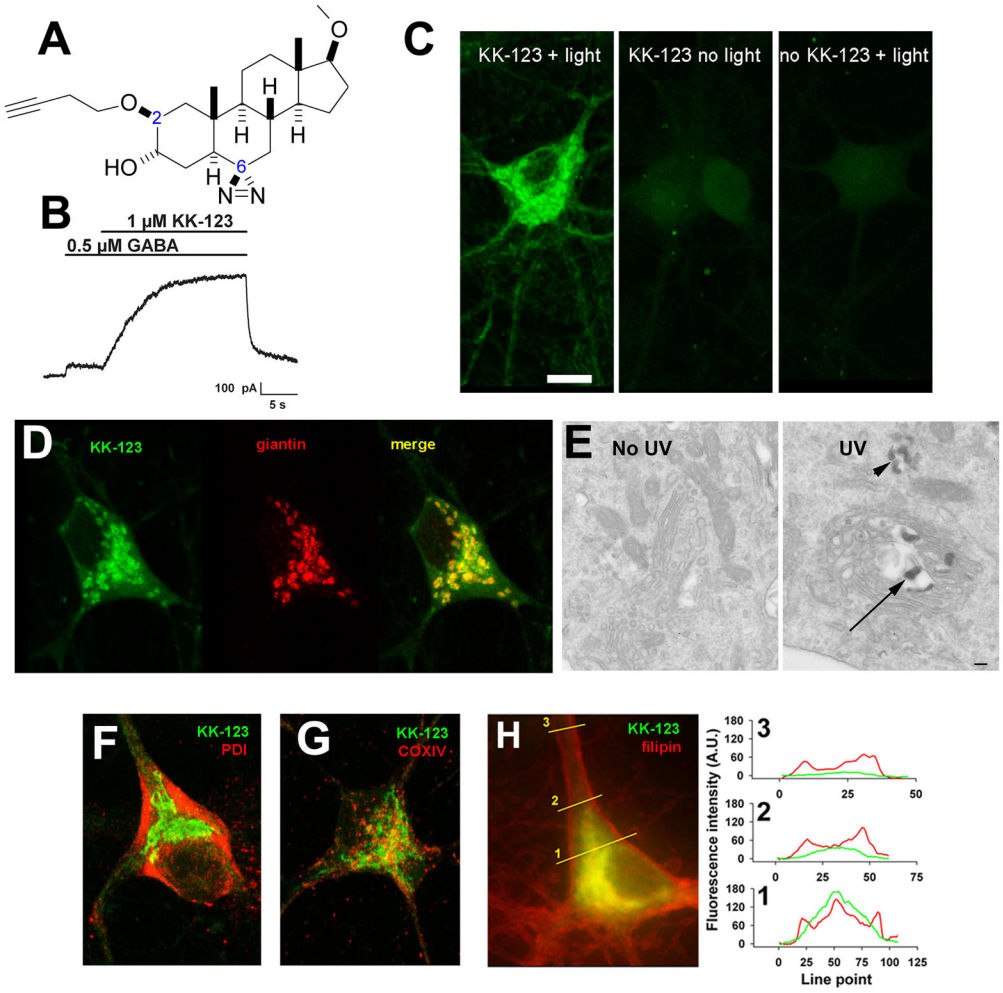

Figure 1.

Golgi-selective labeling of cultured hippocampal neurons by a bi-functional, GABA-active neurosteroid analogue. **A.** Structure of KK-123, showing the alkyne tag (dashed circle) for click chemistry at carbon 2 and the diazirine (dashed rectangle) at carbon 6 for photolabeling. **B.** Potentiation of a GABA activated current in a hippocampal neuron. The neuron was recorded in whole-cell, patch-clamp configuration, filled with a cesium methanesulfonate solution, and clamped at 0 mV. Application of 1 μM KK-123 increased the outward current in response to GABA application. **C.** A hippocampal culture was incubated in 1 μM KK-123 and either exposed to 365 nM UV illumination for 15 min or incubated in the dark, fixed, and processed for click cyto-fluorescence using azide-conjugated AlexaFluor 488. The panels are labeled with the experimental conditions. Only the UV illuminated condition (light) with KK-123 showed significant labeling. **D.** Combined click cyto-fluorescence with immunofluorescence for giantin, a Golgi-specific protein, revealed extensive co-labeling. **E.** Click reaction performed with azide-conjugated biotin, and subsequent processing for electron microscopy (see Methods) revealed reaction product associated with Golgi (arrow) and Golgi-related structures (arrowhead). **F–H.** Little co-localization with the endoplasmic reticulum marker PDI, the mitochondria marker COXIV,

or the fluorescent marker of free membrane cholesterol, filipin. The right panel in H shows line scans of the red (filipin) and green (KK-123) channels to demonstrate partial overlap in labeling, but with KK-123 notably weaker than filipin in plasma-membrane areas, most notable in neurites (line scan 3).

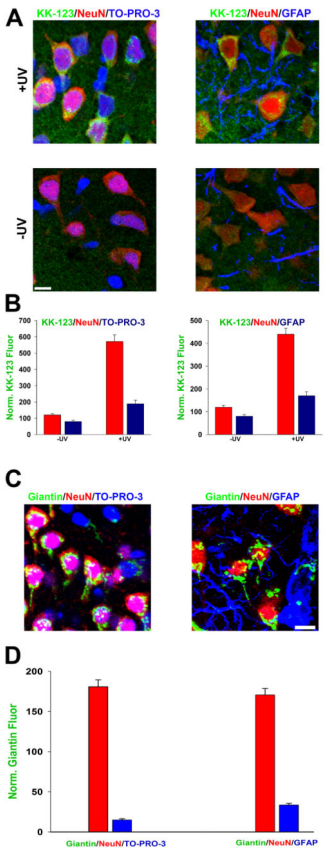

Figure 2.

Selective neuronal labeling is secondary to Golgi accumulation. **A.** In hippocampal slices, KK-123 incubation and click cyto-fluorescence was combined with the NeuN nuclear marker and TO-PRO-3 (left) labeling for all nuclei, including astrocytes. Alternatively, the third marker was a positive label for astrocytes, GFAP. **B.** Quantification of peri-nuclear cytofluorescence of KK-123 in NeuN-positive vs. NeuN-negative cells (blue bars, left panel), or vs. GFAP-positive cells (blue bars, right panel). **C, D.** Images and quantification of peri-nuclear giantin labeling in neurons (red bars) or presumed astrocytes (blue bars).

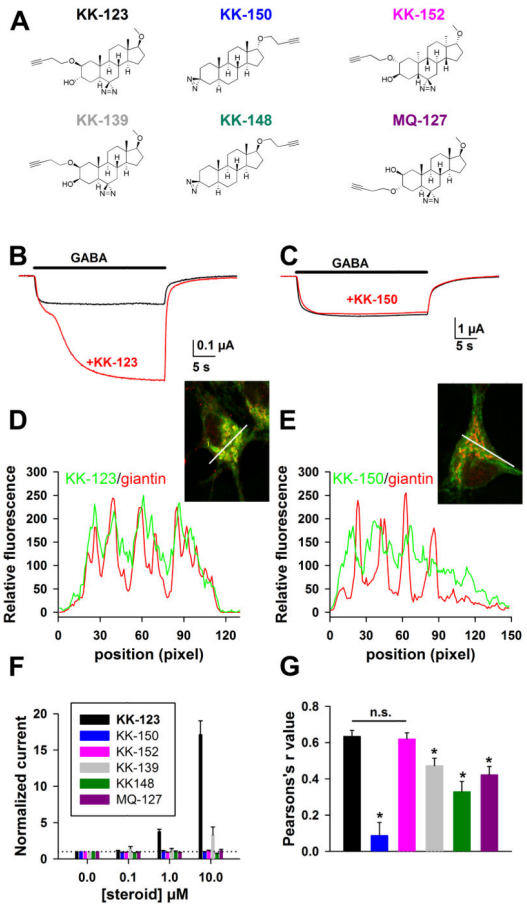

Figure 3.

Altered analogue structure changes Golgi-selective accumulation. **A.** Various structural analogues described in the text. Calculated logP values for the compounds are: KK-123, KK-152, KK-139, and MQ-127: logP = 4.45, KK-148 and KK-150: logP = 6.12. **B, C.** Oocytes expressed $GABA_A$ subunits α1β2γ2L. Responses to GABA showed potentiation in response to co-application of 0.5 μM KK-123 (B) but not in response to co-application of 0.5 μM KK-150. Oocytes were clamped at −70 mV. **D, E.** In neurons, co-localization of KK-123 or KK-150 click cyto-fluorescence (green) and giantin immunolabeling (red) is revealed by a line scan plot of red and green fluorescence intensity. The lines from which the data are derived are shown in the insets. **F.** Summary of potentiation of GABA responses in oocytes at varied compound concentrations. All compounds showed relative inactivity compared with KK-123. MQ-139 exhibited weak but detectable activity at 10 μM (n = 4 oocytes for each compound). Response to GABA alone is denoted by the dotted horizontal reference line. **G.** Summary of co-localization with giantin, reported by Pearsons' r values for compound vs. giantin fluorescence, for all six analogues in neurons (n = 15 cells per condition from 3–4 independent experiments; asterisks indicate $p < 0.05$ after Bonferonni correction for multiple comparisons).

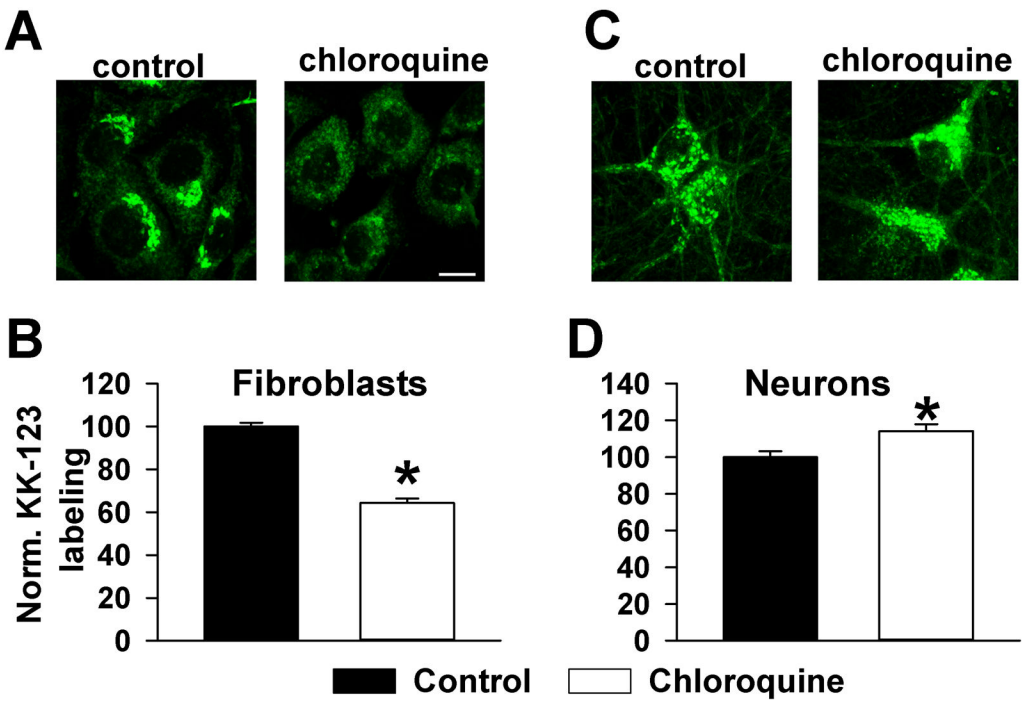

Figure 4.

Cell-selective effect of lysosome disruption, to test a possible endocytic pathway role for Golgi accumulation (Marks and Pagano, 2002). **A, B**. NIH/3T3 cells (fibroblasts) showed chloroquine-sensitive KK-123 accumulation in presumed Golgi. **C, D.** Neurons showed no reduction in KK-123 labeling with the same protocol and in fact a slight increase in labeling intensity. For quantification of fluorescence intensity, regions of interest were placed just outside the nucleus. N = 20–25 cells in 4–5 independent platings.

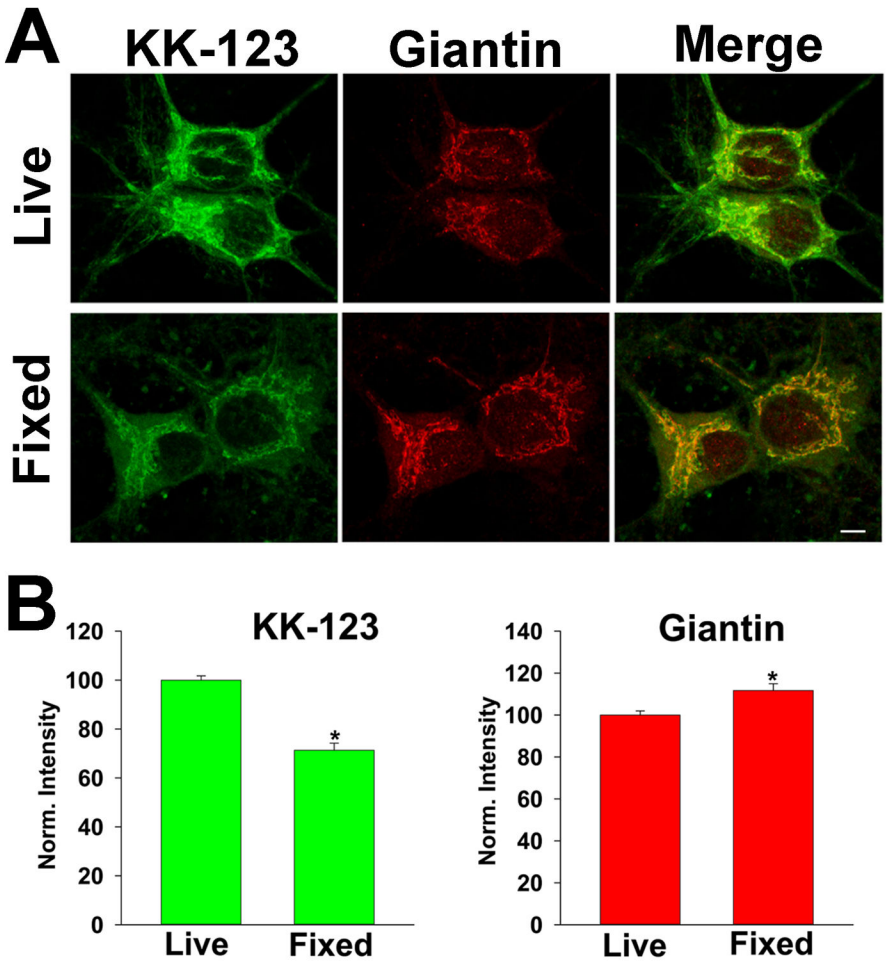

Figure 5.

Golgi-selective accumulation in fixed neurons. **A.** Neurons were incubated in KK-123 and exposed to the UV photolabeling protocol either while alive or after fixation in 4% paraformaldehyde. Live cells were subsequently fixed, then all were processed for click cytofluorescence and immunofluorescence with anti-giantin antibody. **B.** Summary of labeling intensity for the respective signals.

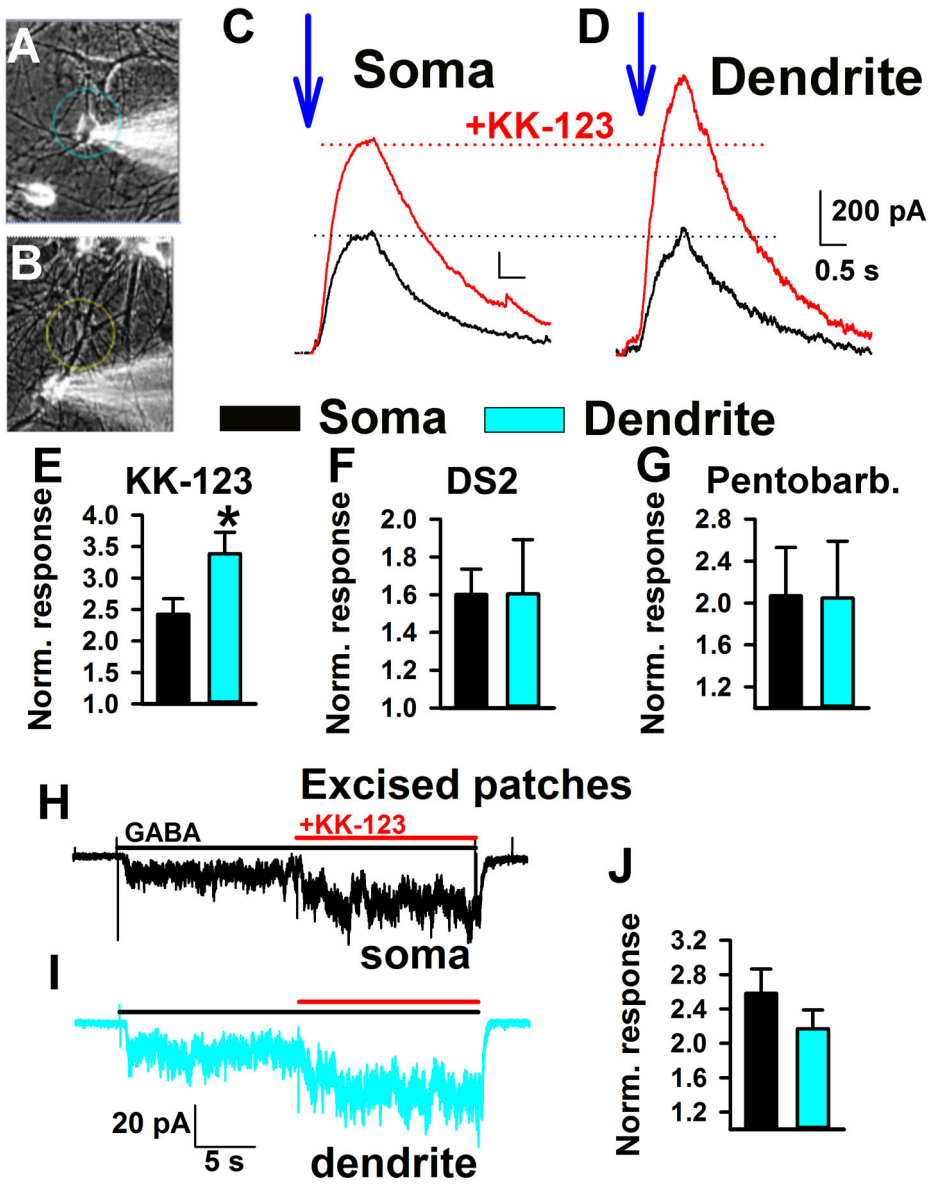

Figure 6.

Weaker steroid effect on somatic inhibition. **A, B.** Photomicrographs depicting the approximate size of uncaging spots on the soma (A) or dendrite (B) in functional studies. Rubi-GABA trimethylphosphine (10 μM) was used as the GABA donor. **C, D.** The blue arrows mark the time of uncaging on soma or dendrite (1 s uncaging duration). GABA responses prior to 0.1 μM KK-123 administration are in black and during KK-123 administration are in red. Currents are displayed scaled to the responses to GABA alone (black traces, dotted black line). Dotted lines show relative increase in potentiation at dendrite relative to soma. The calibration bar labels in D apply also to C. **E–G.** Summary of KK-123 potentiation for soma (black bars, n = 14) and dendrite (blue bars, n = 14) uncaging. All currents were normalized to the response to GABA alone at the same uncaging spot. DS2 (1 μM; n = 9) was used as a δ subunit selective probe. Pentobarbital (20 μM, n = 3; 50

μM, n = 6) was used as a positive allosteric modulator mechanistically similar to neurosteroids. Asterisk indicates $p < 0.05$. **H–J.** Excised patches from somas and dendrites showed indistinguishable potentiation by 100 nM KK-123. GABA was applied at 1 μM. Summary plot shows averages of 9 somatic and 9 dendritic patches.

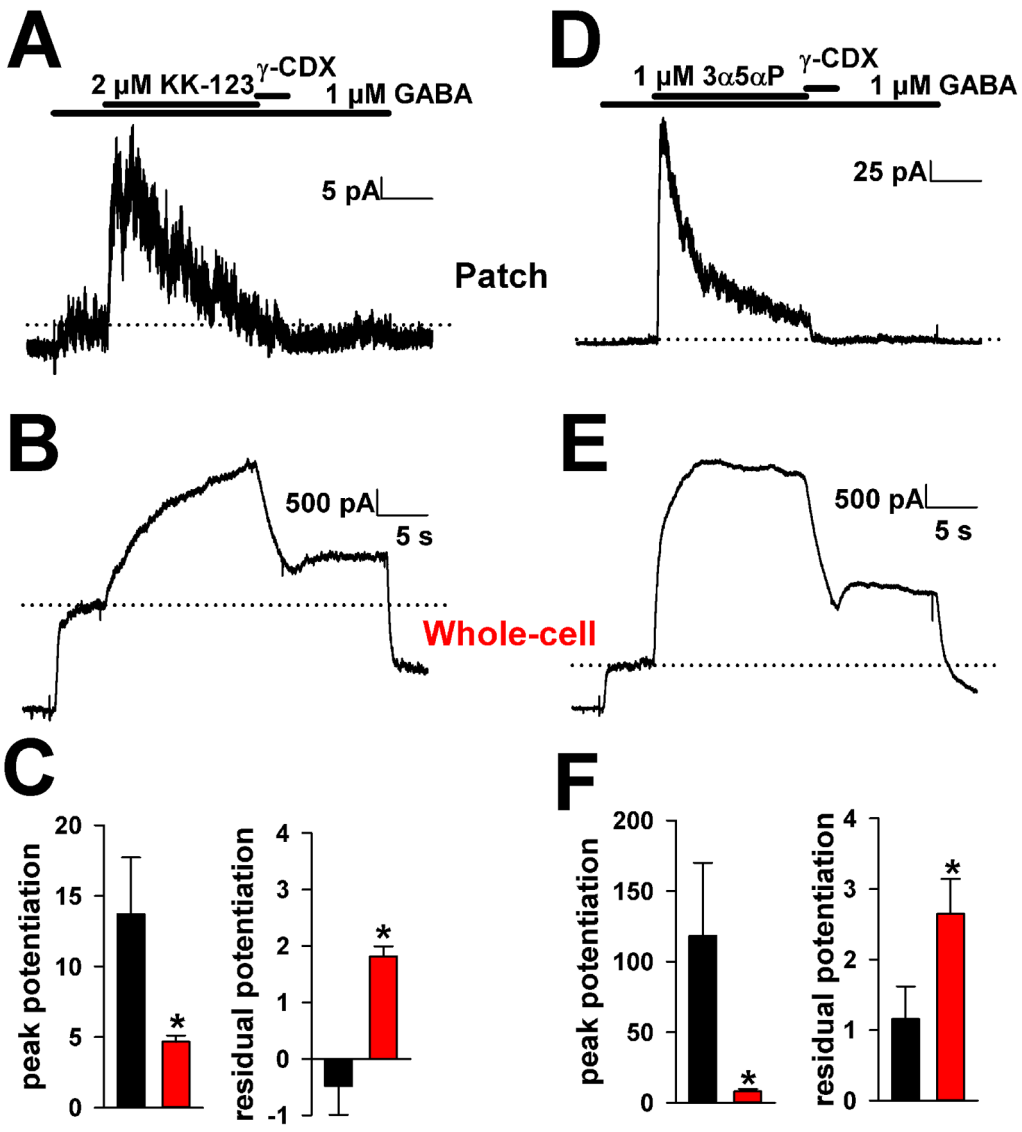

Figure 7.

Differences in steroid responsiveness in excised outside-out patches versus whole-cells. **A–C.** Application of a high concentration of KK-123 showed rapid, strong actions on excised membrane patches and weaker, slower responses in whole-cells. A 3 s γ-cyclodextrin application was insufficient to remove potentiation from whole cells. Residual potentiation was measured 4 s after removal of γ-cyclodextrin. See Supplemental Figure 4 for estimates of perfusion rates onto whole cells. Potentiation is expressed normalized to GABA alone prior to steroid application. In panel C, pooled data from 8 patches (black) and 10 whole cells (red) are shown **D–F.** Similar data for the natural steroid 3α5αP. Asterisks indicate $p < 0.05$.

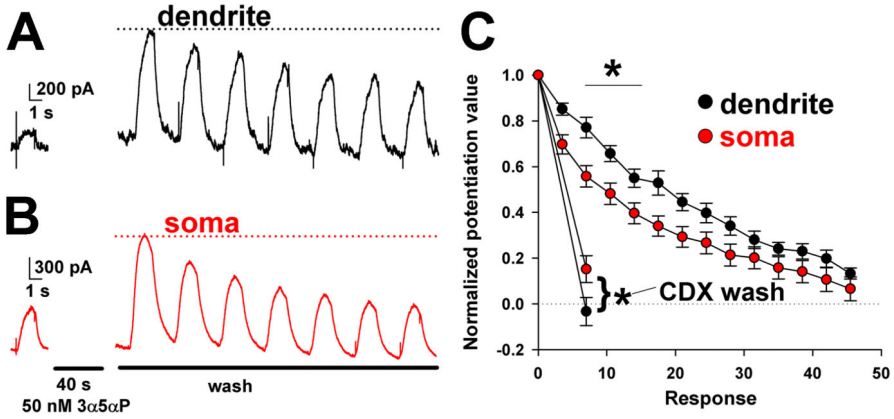

Figure 8.

Faster baseline dissipation of somatic steroid effects; weaker accessibility of somatic steroid effects to extraction. **A, B.** Somatic and dendritic uncaging experiment. Baseline GABA responses are shown on the left. The GABA was applied by uncaging in the continuous presence of Rubi-GABA trimethylphosphine, as in Figure 6. Following steroid (3α5αP) pre-administration by bath perfusion, steroid wash was commenced with saline bath perfusion. Somatic GABA responses returned toward baseline faster than dendritic responses. **C.** Summary of effects from 9 somas and 9 dendrites. In other experiments (separate 9 somas and 9 dendrites), steroid was extracted with membrane impermeant scavenger γ-cyclodextrin (500 μM CDX) applied following the first potentiated response. Dendritic potentiation was returned to baseline (dotted line) more completely than somatic responses. A repeated-measures ANOVA demonstrated an overall difference between dendrites and somas. Asterisks indicate $p < 0.05$ after correction for multiple comparisons.